International Journal of Applied Earth Observation and Geoinformation 52 (2016) 12–19

Contents lists available at ScienceDirect

International Journal of Applied Earth Observation and Geoinformation

journal homepage: www.elsevier.com/locate/jag

3D unmanned aerial vehicle radiation mapping for assessing contaminant distribution and mobility

P.G. Martin[a,*], S. Kwong[b], N.T. Smith[b,e], Y. Yamashiki[c], O.D. Payton[a], F.S. Russell-Pavier[a], J.S. Fardoulis[a], D.A. Richards[d], T.B. Scott[a]

[a] Interface Analysis Centre, HH Wills Physics Laboratory, University of Bristol, Bristol, BS8 1TL, UK
[b] National Nuclear Laboratory, Chadwick House, Warrington, WA3 6AE, UK
[c] Graduate School of Advanced Integrated Studies in Human Survivability, Kyoto University, Kyoto, 606-8501, Japan
[d] School of Geographical Sciences, University of Bristol, Bristol, BS8 1SS, UK
[e] Research Centre for Radwaste and Decommissioning, School of Earth, Atmospheric and Environmental Sciences, Williamson Building, University of Manchester, Manchester, M13 9PL, UK

ARTICLE INFO

Article history:
Received 19 March 2016
Received in revised form 9 May 2016
Accepted 24 May 2016

Keywords:
Fukushima
LiDAR
Radiation mapping
Gamma-spectrometry
Contamination

ABSTRACT

Following the events of March 2011 at the Fukushima Daiichi Nuclear Power Plant, significant quantities of radioactive material were released into the local and wider global environment. At five years since the incident, much expense is being currently devoted to the remediation of a large portion of eastern Japan contaminated primarily by radiocesium, yet further significant expenditure will be required over the succeeding decades to complete this clean-up. People displaced from their homes by the incident are now increasingly keen to return, making it more important than ever to provide accurate quantification and representation of any residual radiological contamination. Presented here is the use of an unmanned aerial vehicle equipped with a laser rangefinder unit to generate a three dimensional point-cloud of an area onto which a radiation contamination map, also obtained concurrently via the unmanned aerial platform, can be rendered. An exemplar site of an un-remediated farm consisting of multiple stepped rice paddy fields with a dedicated irrigation system was used for this work. The results obtained show that heightened radiological contamination exists around the site within the drainage network where material is observed to have collected, having been transported by transient water runoff events. These results obtained in May 2014 suggest that a proportion of the fallout material is highly mobile within the natural environment and is likely to be transported further through the system over the succeeding years.

1. Introduction

The magnitude 9.0 Great Tōhoku earthquake and resulting tsunami that occurred off the eastern coast of Japan in March 2011 (Simons et al., 2011) caused severe damage to three of the four nuclear reactors at the Fukushima Daiichi Nuclear Power Plant (FDNPP). This release was the second largest in history, behind Chernobyl in 1986, being classified at Level 7 (IAEA, 2012), the most major, on the International Nuclear Event Scale (IAEA, 2008) with a release of approximately 520 PBq of activity (Steinhauser et al., 2014). From the releases that occurred over a ten day period, the medium-lived fission product isotopes of cesium, ^{134}Cs and ^{137}Cs, with half-lives of 2.065 and 30.2 years respectively (CRC Press) are the subject of extensive decontamination efforts across a wide area to the west of the Fukushima plant (Hardie and McKinley, 2014; Japanese Ministry of the Environment, 2013; Miyahara et al., 2012; Yasutaka and Naito, 2015).

Over the weeks post release, the extent of the contamination was monitored using a series of high altitude aerial surveys-conducted using manned aircraft at altitudes of 150–700 m (MEXT and United States DoE, 2011; MEXT, 2011). Following these, greater resolution was achieved through the use of unmanned helicopters more commonly used in Japan for agricultural crop-dusting (Sanada and Torii, 2015; Sanada et al., 2014). This technology reduced the pixel resolution to 5 m. Improved resolution over smaller (km^2) areas was achieved by a multirotor unmanned aerial vehicle (UAV) enabling meter-scale mapping of contamination (MacFarlane et al., 2014; Martin et al., 2016). Thus far, this radiation

* Corresponding author.
E-mail address: peter.martin@bristol.ac.uk (P.G. Martin).

http://dx.doi.org/10.1016/j.jag.2016.05.007

surveying work has yielded maps detailing only the 2-dimensional distribution of radiation. Here we explore the use of 3-dimensional mapping as a tool for visualising the location and environmental spread of contamination over a site with extensive local topography. Using such a method, the effects of the site on the spread of radioactivity are rapidly and easily visualised. To generate a 3-dimensional system used within this study, a 2-dimensional radiation map taken of the site is overlain onto a 3-dimensional surface produced by a range-finding system.

In addition to the great effort being devoted to the highly accurate mapping of radiological contamination in the FDNPP fallout zone, many studies have focused on modelling and predicting the movement and eventual fate of radiological contamination within the environment, (Chartin et al., 2013; Masson et al., 2011; Morino et al., 2011) and soils (Kinoshita et al., 2011; Koarashi et al., 2012; Stohl et al., 2012; Tagami et al., 2011; Yasunari et al., 2011). The topographic relief within the contaminated area to the north-west of the plant is sub-mountainous with north-west trending valleys incised with rivers, the largest of which-the Abukuma River, has been the focus of much work to understand the mass transport of material from the catchment (Adhiraga Pratama et al., 2015; Yamashiki et al., 2014) and its eventual deposition out into the neighbouring Pacific Ocean (Buesseler et al., 2011; Masson et al., 2011). The severe typhoon events (June to September) that occur within the region have been shown to be responsible for the movement of significant quantities of material (Chartin et al., 2013; Evrard et al., 2013; Nagao et al., 2013; Yamashiki et al., 2014). In comparison to the climate at Chernobyl, with mean annual precipitation of 621 mm/y (Climate-data.org), Japan's main island (Honshu) is characterised by a monsoon climate with near double mean annual precipitation of 1130 mm/y (Japan Meteorological Agency)—depending on both the distance from the ocean and elevation above sea-level.

LiDAR is defined as a light based "optics remote sensing technology that measures properties of scattered and reflected light to find range and/or other information about a distant target" (Karp and Stotts, 2012). Typical systems use time-of-flight methods whereby the time difference between the laser pulse being sent and received back at the detector corresponds to the distance (or other physical property) based on the speed of light. The majority of systems used currently for cm to m resolution remote sensing over km scales are 3D-scanning LiDAR units; these scanning systems use an array of lasers with discrete pulses at a specific wavelength, each of nanosecond duration, alongside a corresponding array of detectors. Using these scanning systems, it is possible to generate a positional data point-cloud with $\times 10^7$ data points, collected at a rate of 10^5 points per second. This data can be plotted in 3-dimensions to accurately represent (subject to error introducing factors including surface type (Hodgson and Bresnahan, 2004) and atmospheric conditions (Barrett and Ben-Dov, 1967)) for example changes in a topographical surface (Chen et al., 2006), the variance in a tree canopy (Lefsky et al., 2002; Lim et al., 2003; Nilsson, 1996) or mass movement events and subsequent sediment transport (Roering et al., 2009), to produce a digital elevation model or DEM. Within the present work however, distance data from a single-point rangefinder within the detection payload was used. Operating identically in principle to the multi-beam system, but employing only a single beam, firing vertically down from the UAV – the volume of point-cloud data collected to generate a DEM is significantly less, however this sensor still produces a high spatial density of topographic data.

2. Materials and methods

The results described in this study represent the evolution of the unmanned aerial vehicle platform used previously by the authors to monitor contamination within selected field sites across Fukushima Prefecture as well as a former uranium mine in the UK (Martin et al., 2016, 2015). Readers are directed to these works where a comprehensive description and details of the system deployed in this work is provided. A brief summary of the UAV and associated detection system are provided below.

2.1. UAV and data acquisition system

Developed at the University Of Bristol (UK), the aerial system is capable of flights of 30–35 min in duration on lithium polymer batteries. Unlike larger systems, the UAV has a total system weight of 7.0 kg and is capable of carrying a 5.0 kg payload, however to optimise flight time, the total sensing payload weighed only 500 g.

For the radiological survey, the UAV operated following pre-programmed waypoints defined by the operator, with both take-off and landing performed manually using conventional remote controls. Flights were carried out at a consistent ground equivalent speed of 1 ms^{-1}, with the instrument operated at the lowest height safe to do so (typically 1–10 m above the ground surface). A consistent grid spacing of 2.0–2.5 m was maintained during the survey to ensure adequate ground coverage.

As with previous works, the radiation detection payload used within this study featured a miniature gamma-ray spectrometer, produced by Kromek™ (Co. Durham, UK). The uncollimated, small volume (1 cm^3), cadmium zinc telluride (CZT) co-planar grid spectrometer has an energy range of 30 keV to 3.0 MeV, with an energy resolution of <2.5% @ 662 keV. Electrical noise within the detector was <10 keV Full Width at Half Maximum (FWHM) (Kromek Group PLC, 2015). Mounted next to the radiation detector on a three-axis gyro-stabilised gimbal was a single-point laser rangefinder with an accuracy of ±5 cm over the 0.2–30 m instrumental range, operating at a wavelength of 905 nm (near-infrared) (AR2500 Acuity™).

Data from both the gamma-spectrometer and rangefinder were sampled every 500 ms, with the values recorded onto a small microcontroller (Arduino ADK, Scarmagno, Italy) alongside a GPS location sampled from an on-board antenna.

2.2. Survey site

The site chosen for the study was a stepped farmstead within the Kawamata region of Fukushima prefecture (N 37°35.1154′, E 140°42.0781′) (Fig. 1) located near to the eastern border with Namie, contaminated as an effect of the north-west trending plume released from the FDNPP. A recent report by the Ministry of Economy, Trade and Industry (METI) labelled the site, 35 km from as plant, and the surrounding region as an area "in which residents are not permitted to live". To the north of the stepped fields, at the highest point on the site, there exists a small house with gently sloping roofs that have been previously characterised using a UAV (Martin et al., 2016). The contaminated ground studied was a strip 200 × 50 m running north-south, formed of a series of smaller gently inclined fields of varying sizes-with the southern limit of each of these fields bounded by a shallow water-filled drainage ditch approximately 30 cm in depth. To the south of each of these ditches, forming the vertical steps throughout the site, were a series of steeply inclined, near vertical banks, ranging from 1 to 5 m in height. This site in Irikuboyama (Kawamata) was also selected due to its proximity to an existing JAEA test site (Higashikuboyama) examining the distribution of radioactive substances discharged by the Fukushima incident (MEXT and NRA, 2012, 2013). Work at this location, and other similar sites along the plume profile, sought to investigate the retention of ^{134}Cs and ^{137}Cs within differing soil profiles as well as within differing crop types.

Previous work by Abe et al. (1981), investigating the background levels of radiation across the entirety of Japan with respect to

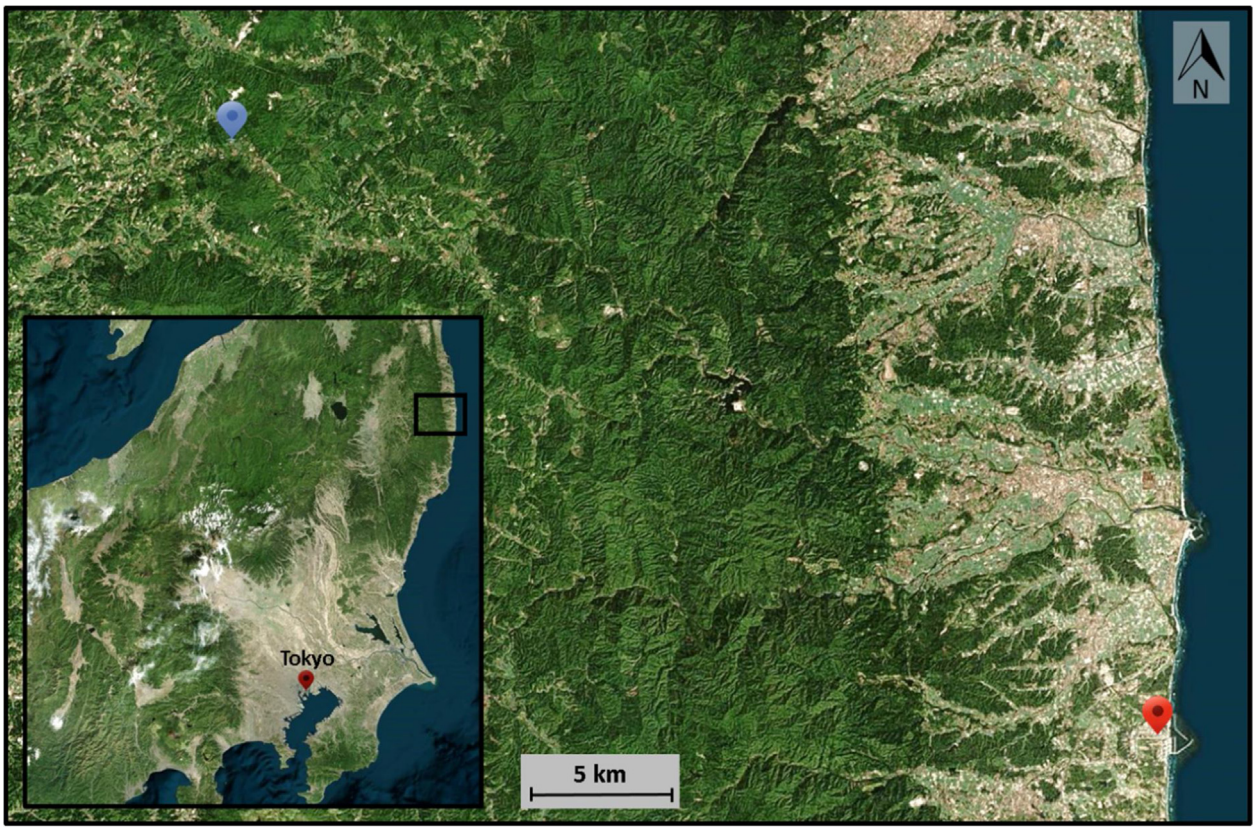

Fig. 1. Map of eastern Japan showing the location of both the Fukushima Daiichi Nuclear Power Plant (FDNPP) [red] and the survey site [blue]. (© Bing Maps) (For interpretation of the references to colour in this figure legend, the reader is referred to the web version of this article.)

influences from both the sub-surface geology and atmospheric fallout determined average values of 0.097 ± 0.013 and 0.09 μSv/h for Fukushima Prefecture and Japan as a whole respectively. Due to its very low level, and highly homogenous nature, this work assumes that the impact from this background radioactivity on the results obtained in this radiological survey are constant and can be considered negligible with respect to the levels determined in this work.

Using both the altitude of the UAV recorded by the on-board GPS and the distance to the ground produced from the single point laser rangefinder (Fig. 2), it was possible to generate a plot of the topography of the land surface. Onto this digital elevation model (DEM), the results from radiological mapping were applied.

2.3. Data analysis

Custom software was produced to complement existing software platforms. Maps of radiation intensity were plotted detailing radiation levels (in counts per second (CPS)) as a coloured scaling overlain onto a base map over the entire measurable energy range of the detector (30 keV–3.0 MeV) normalised to a height of 1 m using data from the laser rangefinder. As in previous works, this normalisation was conducted with the possible source area on the ground existing as a function of the horizontal aperture of the detector and its altitude, following an inverse-square law calculation of radiation dispersion originating from a point source.

In order to construct a DEM within geospatial analysis software, additional software was produced to convert the raw data from the UAV system into the XML file format. The data outputted consisted of longitude and latitude arrays as well as values for CPS and ground surface height (calculated from the difference between the GPS altitude and distance to the surface measured with the rangefinder).

2.4. 3-Dimensional visualisation model

Using the data exported from the analysis software, construction of the 3-dimensional radiation model was conducted using the UK National Nuclear Laboratory (NNL) prototype "EnVi" (**En**vironmental **Vi**sualisation, a 3D digital data pre-processor) software which was designed in-house to enable visualisation of 3D spatial data with attributes, such as aerial LiDAR and radiation data collected from instrument platforms such as the UAV deployed in this study. The utility was developed using Visual Basic for Applications (VBA) (Microsoft Corporation) for data originating from Excel™ or text file formats. Traditional geographical information system (GIS) analysis techniques are often utilised to create a 3D view of attributes such as population densities, vegetation and land temperature. However, these traditionally rely on the production of a DEM from the LiDAR's 3D point cloud dataset, creation of a gridded surface from the dataset being mapped in 3D (typically requiring accompanying GPS measurements for each measurement) and then the draping of the attribute surface onto the 3D surface. This creates problems/inconsistency when one dataset is georeferenced to its 3D counterpart (Naoum et al., 2005), particularly if the grid points are slightly offset during gridding operations. Draping of the attribute grid over the 3D grid can result in inaccuracies in the translation of the 2D point onto the 3D surface.

EnVi uses the points in the 3D dataset with attributes directly. Data visualisation is achieved in a two stage process. Firstly, triangular cells are created (using all data points) over the whole observed domain using Delaunay triangulation. Secondly, contour-

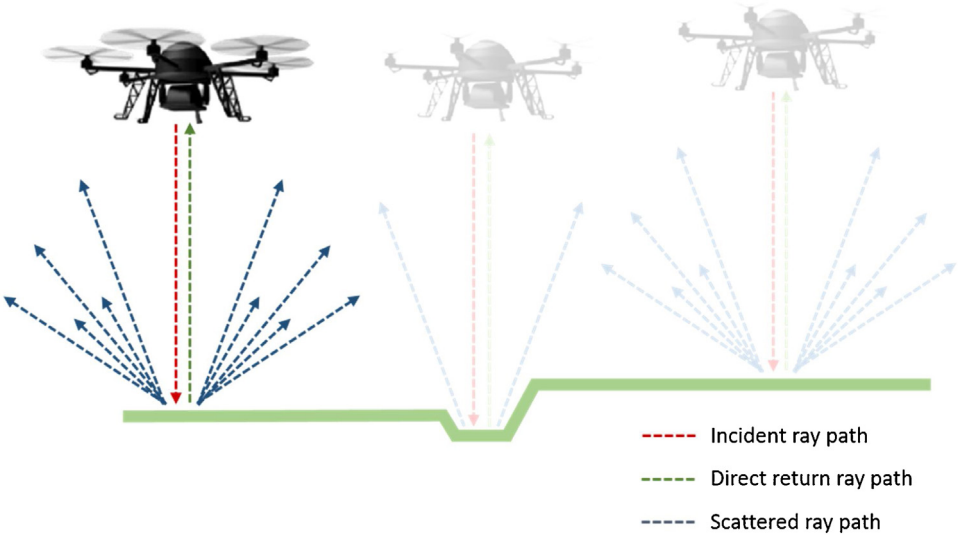

Fig. 2. Diagrammatic representation of the use of a single-point rangefinder coupled with GPS altitude to derive a highly accurate elevation model of a site; onto which radiation data can be overlain.

ing of the attribute is performed over all the triangular cell surfaces to produce a 3D image of the selected attribute.

In this study, visualisation is provided by the open source software Paraview™. Traditional GIS analysis relies on the use of a georeferenced coordinate system, but EnVi utilises the data points themselves to create its own coordinate system. The direct use of data points (with spatial and attributes information) by EnVi eliminates the need for time-consuming creation of several surfaces prior to the manual draping operations often adopted in GIS systems. This processing efficiency therefore allows for a quicker 3D visualisation of surfaces in the field, effectively in real-time, a useful feature for situations such as following the radioactive releases from Fukushima.

3. Results and discussion

Following the release from the Fukushima Daiichi Nuclear Power Plant in March 2011, studies have estimated the deposition of radiocesium to be largely uniform, with a homogenous covering of 1–2 MBq/m^2 across the affected study area (MEXT, 2011), as also approximated in Malins et al., 2016. However, over the thirty eight months between the radioactive release and the airborne survey in May 2014, regions of evolving differential radioactivity are observed at the meter scale.

A map detailing the course (X, Y co-ordinates) taken by the UAV in mapping the site is shown in Fig. 3 (a), with the corresponding plot of radiological contamination (normalised to 1 m) in Fig. 3 (b). Apparent within the inclined site is the substantial variation in recorded radioactivity over the duration of the survey. At both the top and bottom limits of the north-south trending property are regions with reduced activity when compared to other parts of the site. The northern and southernmost areas display typical activities of between 80 and 100 CPS (1.3–1.5 μSv/h), considerably less than the 300–320 CPS (4.7–5.1 μSv/h) found centrally within the site.

These isolated regions with heightened activity likely represent natural pre-concentration, whereby movement of fallout particles due to fluid flow downslope has transported the material where it had, at the time of the radiation survey, been deposited. The gamma-ray spectra produced from the region in the north portion of the site highlighted in Fig. 3 (a) is presented in Fig. S1, showing the non-natural contribution from radiocesium (^{134}Cs and ^{137}Cs).

In order for the rangefinder data to be used to construct the DEM, the effects of different thicknesses of water over the site causing irregular pulse returns had to be considered. The results of in-lab experiments are presented within Fig. 4. At low thicknesses of water (up to 0.4 m), a consistent return is observed-with the measured height equalling the true height the system was above the ground. However, at greater water depths (>0.5 m) the values produced by the rangefinder for measured distances are not equal to the true distance-this is believed to be due to the piling-up of the various returns travelling back to the rangefinder from the water and container surfaces. To account for any such erroneous contributions to the recorded elevation model, outlier points were removed through nearest neighbour comparison of returns.

Through processing of the data captured by the UAV, it was possible to generate an accurate terrain DEM of the site, shown in Fig. 5 (a). Illustrated is the marked variation in height across the site progressing from south to north. The stepped nature of the site is apparent in the DEM produced by the rangefinder. A total elevation change of 31.5 m over the 215 m length of the farmstead represents a moderate gradient of 14.6%.

Results of applying the processed radiation intensity map (Fig. 5 (b)) to the elevation model are shown in Fig. 5 (c). From these radiation maps, the locations of most significant contaminant accumulations coincide within small local topographical low points on the site. Such areas correspond to the location of the drainage network at the southern end of each of the individual flat stepped fields.

With radioactive material having originally likely been deposited uniformly over the site, this survey strongly indicates that material has been transported and redistributed under the action of downward water flow, having been subsequently deposited where momentum no longer permits transport. The low levels of radiation from the higher ground to the west of the site also likely corresponds to the transport of material away from where it was originally deposited. Extensive work has previously used the deposition and transportation of caesium from natural sources (Walling and Quine, 1991) as well as following nuclear testing (De Jong et al., 1983; Longmore et al., 1983) as a method for analysing soil erosion and transportation.

Based on the contaminant migration occurring over the 38 months from March 2011 to May 2014, this work supports other previous studies reporting contaminant mobility, suggesting that

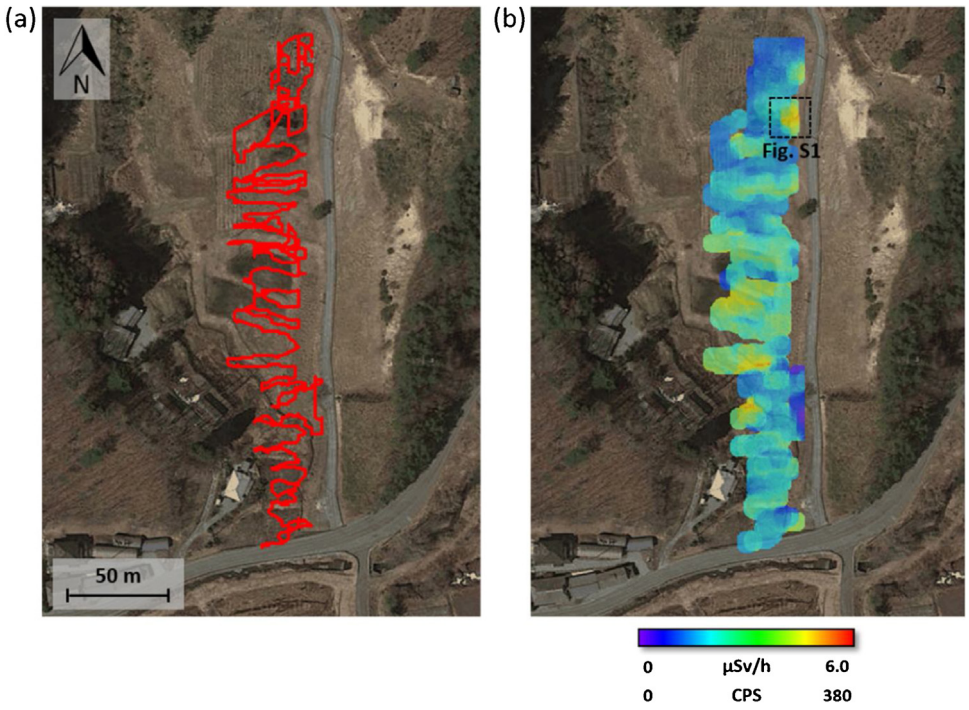

Fig. 3. (a) Flight path of the UAV undertaken during the site survey and (b) corresponding radiation distribution map with detected values normalised to 1 m above the ground surface. The location of the gamma-ray spectrum presented in Fig. S1 is shown.

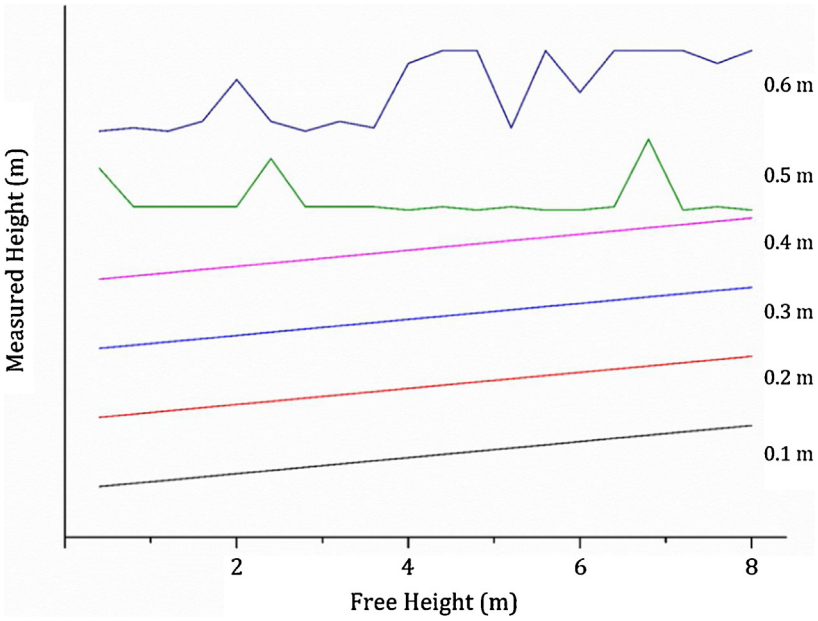

Fig. 4. Response of the range-finding LiDAR at varying altitudes to differing thicknesses of water—a marked change in response is observed at greater fluid thickness.

the material ejected from the FDNPP is mobile within the environment absorbed onto the surfaces of microscopic clay particles. This material is then readily transported through frequent meteoric events. It is anticipated that the downslope spread of contamination will continue indefinitely until it accumulates within the lowest local topographical minima within the landscape or enters streams and rivers flowing eastwards towards the coast and the Pacific Ocean; the mountainous terrain of the areas affected by the radioactive releases will likely increase the rate at which this migration will occur. Research following the Chernobyl accident by Rosén et al. (1999) found the retention of caesium within the ground to be strong, with material remaining in the uppermost soil horizons. A later comparison of both the Chernobyl and Fukushima radiocesium behaviour by Konoplev et al. (Konoplev et al., 2016) examined numerous environmental properties including the partition coefficient (K_d). The work concluded that the K_d value of the radiocesium from Fukushima is 1–2 orders of magnitude greater than that observed within the Chernobyl zone; this is attributed to the high radiocesium interception potential (RIP) as a factor of the high clay content of the Fukushima soil as well as the insoluble and glassy nature of the fallout (Adachi et al., 2013). Konoplev et al. also found that the normalised dissolved wash-off coefficients

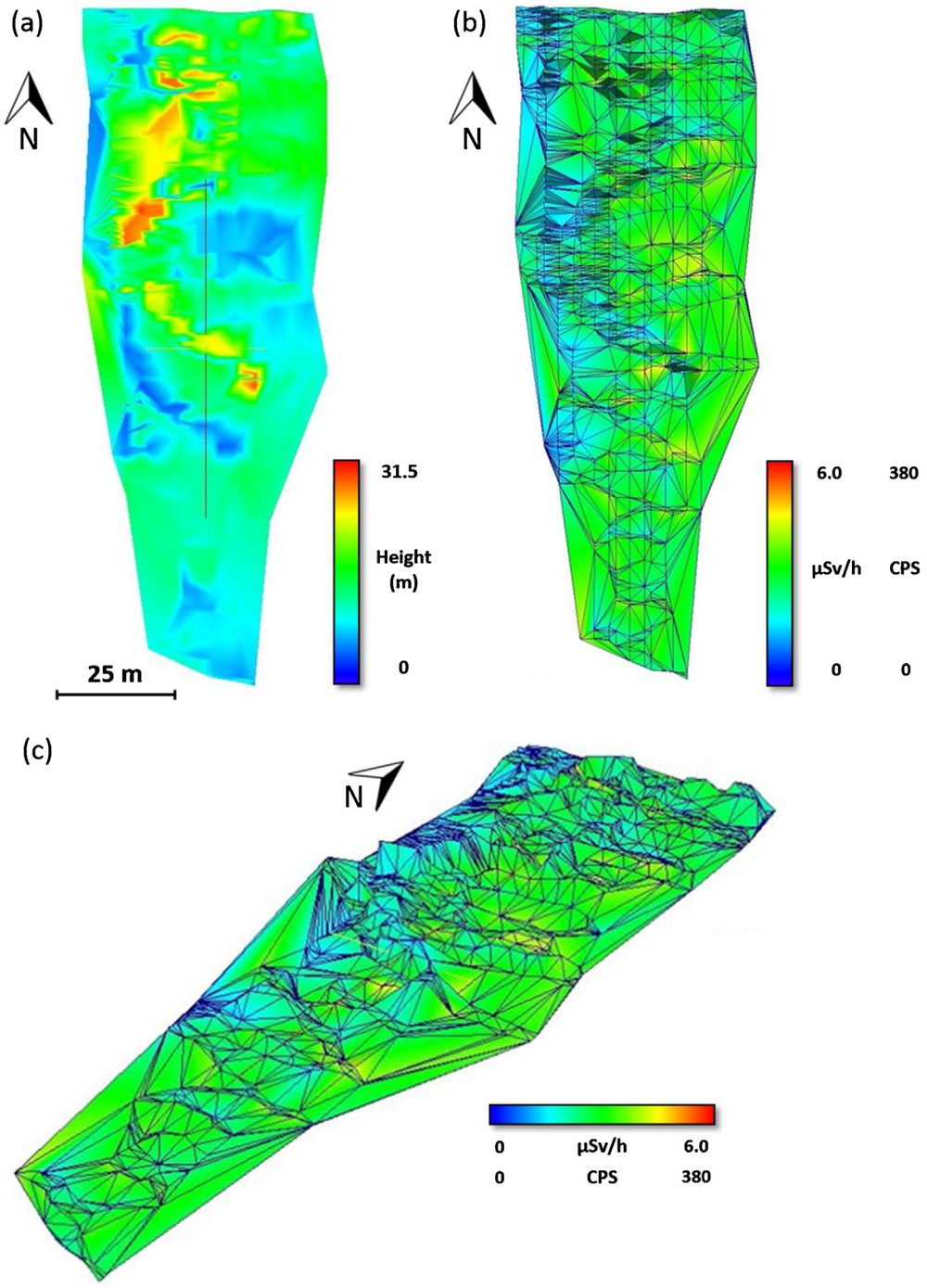

Fig. 5. (a) Elevation model of the site shaded for height above ground, (b) wire-frame model overlain with counts per second and dose rate data and (c) three-dimensional site model showing altitude overlain with radiation intensity data.

for Fukushima catchments are 1–2 orders of magnitude lower than Chernobyl, whereas the normalised particle wash-out coefficients were comparable for both localities. In addition to the differing soil properties, the greater volume of annual precipitation and frequent severe weather events may also be associated with an enhanced mobility of radiocesium.

4. Conclusions and future work

Through the use of unmanned aerial vehicles equipped with both radiation detection and laser range-finding systems it was possible to construct a highly accurate model of a 1000 m^2 stepped farmstead within the fallout affected Kawamata Town region of Fukushima prefecture. With both detectors mounted on the same payload unit, recording at a frequency of 2 Hz, a single survey flight of 15 min was enough to capture all the data presented within this work.

With respect to the clean-up operation currently ongoing within the region, this work highlights the useful application of such a 3D mapping system—in near real-time illustrating the movement of contamination on the meter scale. Despite efforts of the Japanese authorities who have since remediated this farmstead through the removal of the uppermost 10 cm of material, the continual addition of new contaminant material from greater heights to the north of

this site will likely contribute to the case for further remediation activity in the future.

Future work on the system will seek to apply a 32 laser, 3D-scanning LiDAR system in addition to the standard radiation detection payload for the construction of super high-resolution three dimensional radiation maps of structures such as buildings and waste material storage sites for both monitoring and visualising contamination. The utilisation of high-performance computing will allow for the potential ray-tracing and construction of highly accurate radiation models to pinpoint the origin of such contamination. As well as forming a potential role within disaster recovery, the use of high-resolution three-dimensional radiation mapping may be highly useful for more general nuclear decommissioning and post-operational clean-out.

Acknowledgements

The authors wish to thank the University of Bristol for funding the fieldwork in association with the institutional strategic alliance with Kyoto University. Additional thanks are extended to Sellafield Ltd., Kromek Ltd., University of Bristol Cabot Institute and the University of Bristol's Physics workshop. Smith is funded by a Royal Society Industry Fellowship. Smith and Kwong also thank NNL Environmental Services for their support. Impact Acceleration funding for the development of the system was provided by the Engineering and Physical Sciences Research Council (EPSRC) (Grant number: EP/K503824/1).

Appendix A. Supplementary data

Supplementary data associated with this article can be found, in the online version, at http://dx.doi.org/10.1016/j.jag.2016.05.007.

References

Abe, S., Fujitaka, K., Abe, M., Fujimoto, K., 1981. Extensive field survey of natural radiation in Japan. J. Nucl. Sci. Technol. 18 (1), 21–45, http://dx.doi.org/10.1080/18811248.1981.9733221.

Adachi, K., Kajino, M., Zaizen, Y., Igarashi, Y., 2013. Emission of spherical cesium-bearing particles from an early stage of the Fukushima nuclear accident. Sci. Rep. 3, 2554, http://dx.doi.org/10.1038/srep02554.

Adhiraga Pratama, M., Yoneda, M., Shimada, Y., Matsui, Y., Yamashiki, Y., 2015. Future projection of radiocesium flux to the ocean from the largest river impacted by Fukushima Daiichi Nuclear Power Plant. Sci. Rep. 5, 8408, http://dx.doi.org/10.1038/srep08408.

AR2500 Acuity™ (n.d.). Acuity AR2500 Specification. Retrieved June 3, 2015, from www.acuitylaser.com.

Barrett, E.W., Ben-Dov, O., 1967. Application of the lidar to air pollution measurements. J. Appl. Meteorol. 6 (3), 500–515, http://dx.doi.org/10.1175/1520-0450(1967)006<0500:AOTLTA>2.0.CO;2.

Buesseler, K., Aoyama, M., Fukasawa, M., 2011. Impacts of the Fukushima nuclear power plants on marine radioactivity. Environ. Sci. Technol. 45 (23), 9931–9935, http://dx.doi.org/10.1021/es202816c.

Chartin, C., Evrard, O., Onda, Y., Patin, J., Lefèvre, I., Ottlé, C., . . . Bonté, P., 2013. Tracking the early dispersion of contaminated sediment along rivers draining the Fukushima radioactive pollution plume. Anthropocene 1, 23–34, http://dx.doi.org/10.1016/j.ancene.2013.07.001.

Chen, R.-F., Chang, K.-J., Angelier, J., Chan, Y.-C., Deffontaines, B., Lee, C.-T., Lin, M.-L., 2006. Topographical changes revealed by high-resolution airborne LiDAR data: the 1999 Tsaoling landslide induced by the Chi–Chi earthquake. Eng. Geol. 88 (3–4), 160–172, http://dx.doi.org/10.1016/j.enggeo.2006.09.008.

Climate of Pripyat. Retrieved January 14, 2016, from http://pt.climate-data.org/location/715182/.

CRC Press, 2015. CRC Handbook of Chemistry and Physics—Table of Isotopes. In: M. Haynes, W. (Ed.), 96th ed. Boca Raton, Florida (Retrieved from) http://www.hbcpnetbase.com/.

De Jong, E., Begg, C.B.M., Kachanoski, R.G., 1983. Estimates of soil erosion and deposition for some Saskatchewan soils. Can. J. Soil Sci. 63 (3), 607–617, http://dx.doi.org/10.4141/cjss83-061.

Evrard, O., Chartin, C., Onda, Y., Patin, J., Lepage, H., Lefèvre, I., Bonté, P., 2013. Evolution of radioactive dose rates in fresh sediment deposits along coastal rivers draining Fukushima contamination plume. Sci. Rep. 3, 3079, http://dx.doi.org/10.1038/srep03079.

Hardie, S.M.L., McKinley, I.G., 2014. Fukushima remediation: status and overview of future plans. J. Environ. Radioact. 133, 75–85, http://dx.doi.org/10.1016/j.jenvrad.2013.08.002.

Hodgson, M., Bresnahan, P., 2004. Accuracy of airborne LIDAR-derived elevation. Photogramm. Eng. Remote Sens. (Retrieved from) http://www.ingentaconnect.com/content/asprs/pers/2004/00000070/00000003/art00005.

IAEA, 2008. The International Nuclear and Radiological Event Scale User's Manual. Vienna, Austria: International Atomic Energy Agency. Retrieved from http://www-pub.iaea.org/MTCD/Publications/PDF/INES2013web.pdf.

IAEA, 2012. Re-evaluation of INES rating; Effect to the Nuclear Facilities from the earthquake on east area of Japan. NEWS: The Information Channel on Nuclear and Radiological Events. Vienna. Retrieved from https://www-news.iaea.org/ErfView.aspx?mId=b8d002ae-78cc-435b-a9c6-21860bdb46cc.

Japan Meteorological Agency. (n.d.). Monthly total of precipitation (mm)—Japan Meteorological Agency. Retrieved January 14, 2016, from http://www.data.jma.go.jp/obd/stats/etrn/view/monthly_s3_en.php?block_no=47401&view=13.

Japanese Ministry of the Environment, 2013. Decontamination Guidelines, 2nd Edition 2013. Retrieved from http://josen.env.go.jp/en/framework/pdf/decontamination_guidelines_2nd.pdf.

Karp, S., Stotts, L., 2012. Fundamentals of Electro-optic Systems Design: Communications, Lidar, and Imaging. Retrieved from https://books.google.co.uk/books?hl=en&lr=&id=NYqFMOM6MRgC&oi=fnd&pg=PR11&dq=Karp+and+Stotts+2012&ots=JWo8Yfb_c-&sig=5yFDZIfVsk6VrFV5WVe9aiFA-6U.

Kinoshita, N., Sueki, K., Sasa, K., Kitagawa, J., Ikarashi, S., Nishimura, T., Yamagata, T., 2011. Assessment of individual radionuclide distributions from the Fukushima nuclear accident covering central-east Japan. Proc. Natl. Acad. Sci. U. S. A. 108 (49), 19526–19529, http://dx.doi.org/10.1073/pnas.1111724108.

Koarashi, J., Atarashi-Andoh, M., Matsunaga, T., Sato, T., Nagao, S., Nagai, H., 2012. Factors affecting vertical distribution of Fukushima accident-derived radiocesium in soil under different land-use conditions. Sci. Total Environ. 431, 392–401, http://dx.doi.org/10.1016/j.scitotenv.2012.05.041.

Konoplev, A., Golosov, V., Laptev, G., Nanba, K., Onda, Y., Takase, T., Yoshimura, K., 2016. Behavior of accidentally released radiocesium in soil–water environment: looking at Fukushima from a Chernobyl perspective. J. Environ. Radioact. 151, 568–578, http://dx.doi.org/10.1016/j.jenvrad.2015.06.019.

Kromek Group PLC, 2015. GR1 Spec Sheet; Revision 10. Retrieved June 23, 2015, from http://www.kromek.com/products_gr1spectrometer.asp.

Lefsky, M.A., Cohen, W.B., Parker, G.G., Harding, D.J., 2002. Lidar remote sensing for ecosystem studies. Bioscience 52 (1), 19, http://dx.doi.org/10.1641/0006-3568(2002)052[0019:LRSFES]2.0.CO;2.

Lim, K., Treitz, P., Wulder, M., St-Onge, B., Flood, M., 2003. LiDAR remote sensing of forest structure. Prog. Phys. Geogr. 27 (1), 88–106, http://dx.doi.org/10.1191/0309133303pp360ra.

Longmore, M., O'leary, B., Rose, C., Chandica, A., 1983. Mapping soil erosion and accumulation with the fallout isotope caesium-137. Soil Res. (Retrieved from) http://www.publish.csiro.au/paper/SR9830373.

MacFarlane, J.W., Payton, O.D., Keatley, A.C., Scott, G.P.T., Pullin, H., Crane, R.A., Scott, T.B., 2014. Lightweight aerial vehicles for monitoring, assessment and mapping of radiation anomalies. J. Environ. Radioact. 136, 127–130, http://dx.doi.org/10.1016/j.jenvrad.2014.05.008.

Malins, A., Kurikami, H., Nakama, S., Saito, T., Okumura, M., Machida, M., Kitamura, A., 2016. Evaluation of ambient dose equivalent rates influenced by vertical and horizontal distribution of radioactive cesium in soil in Fukushima Prefecture. J. Environ. Radioact. (Pt. 1), 38–49, http://dx.doi.org/10.1016/j.jenvrad.2015.09.014.

Martin, P.G., Payton, O.D., Fardoulis, J.S., Richards, D.A., Scott, T.B., 2015. The use of unmanned aerial systems for the mapping of legacy uranium mines. J. Environ. Radioact. 143, 135–140, http://dx.doi.org/10.1016/j.jenvrad.2015.02.004.

Martin, P.G., Payton, O.D., Fardoulis, J.S., Richards, D.A., Yamashiki, Y., Scott, T.B., 2016. Low altitude unmanned aerial vehicle for characterising remediation effectiveness following the FDNPP accident. J. Environ. Radioact. 151, 58–63, http://dx.doi.org/10.1016/j.jenvrad.2015.09.007.

Masson, O., Baeza, A., Bieringer, J., Brudecki, K., Bucci, S., Cappai, M., Zhukova, O., 2011. Tracking of airborne radionuclides from the damaged Fukushima Dai-ichi nuclear reactors by European networks. Environ. Sci. Technol. 45 (18), 7670–7677, http://dx.doi.org/10.1021/es2017158.

MEXT, 2011. Results of the Airborne Monitoring by the Ministry of Education, Culture, Sports, Science and Technology and the U.S. Department of Energy. 6th May 2011. Retrieved from http://radioactivity.nsr.go.jp/en/contents/4000/3180/24/1304797_0506.pdf.

MEXT & NRA, 2012. Results of the Research on Distribution of Radioactive Substances Discharged by the Accident at TEPCO's Fukushima Dai-ichi *NPP*. Retrieved from http://radioactivity.nsr.go.jp/en/contents/1000/294/24/PressR040802.pdf.

MEXT & NRA, 2013. Depth Distribution of Radioactive Substances in Model Area Soil in the Distribution Survey of Radioactive Substances. Retrieved from http://emdb.jaea.go.jp/emdb/en/portals/b212/.

MEXT & United States DoE, 2011. Results of Airborne Monitoring by the Ministry of Education, Culture, Sports, Science and Technology and the U.S. Department of Energy. Retrieved from http://radioactivity.nsr.go.jp/en/list/307/list-1.html.

Miyahara K., Tokizawa T., Nakayama S., 2012. Overview of the Results of Fukushima Decontamination Pilot Projects. IAEA International Expertsí Meeting on Decommissioning and Remediation after a Nuclear Accident. Retrieved from http://www-pub.iaea.org/iaeameetings/IEM4/30Jan/Miyahara.pdf.

Morino, Y., Ohara, T., Nishizawa, M., 2011. Atmospheric behavior, deposition, and budget of radioactive materials from the Fukushima Daiichi nuclear power

plant in March 2011. Geophys. Res. Lett. 38 (7), http://dx.doi.org/10.1029/2011GL048689, n/a–n/a.
Nagao, S., Kanamori, M., Ochiai, S., 2013. Export of 134 Cs and 137 Cs in the Fukushima river systems at heavy rains by Typhoon Roke in September 2011. Biogeosciences, http://dx.doi.org/10.5194/bg-10-6215-2013.
Naoum, S., Tsanis, I.K., Fullarton, M., 2005. A GIS pre-processor for pollutant transport modelling. Environ. Modell. Software 20 (1), 55–68, http://dx.doi.org/10.1016/j.envsoft.2003.12.009.
Nilsson, M., 1996. Estimation of tree heights and stand volume using an airborne lidar system. Remote Sens. Environ. 56 (1), 1–7, http://dx.doi.org/10.1016/0034-4257(95)00224-3.
Roering, J.J., Stimely, L.L., Mackey, B.H., Schmidt, D.A., 2009. Using DInSAR, airborne LiDAR, and archival air photos to quantify landsliding and sediment transport. Geophys. Res. Lett. 36 (19), L19402, http://dx.doi.org/10.1029/2009GL040374.
Rosén, K., Öborn, I., Lönsjö, H., 1999. Migration of radiocaesium in Swedish soil profiles after the Chernobyl accident, 1987–1995. J. Environ. Radioact. 46 (1), 45–66, http://dx.doi.org/10.1016/S0265-931X(99)00040-5.
Sanada, Y., Kondo, A., Sugita, T., Nishizawa, Y., Youichi, Y., Kazutaka, I., Torii, T., 2014. Radiation monitoring using an unmanned helicopter in the evacuation zone around the Fukushima Daiichi nuclear power plant. Explor. Geophys., Retrieved from http://library.seg.org/doi/abs/10.1071/EG13004.
Sanada, Y., Torii, T., 2015. Aerial radiation monitoring around the Fukushima Dai-ichi Nuclear Power Plant using an unmanned helicopter. J. Environ. Radioact. 139, 294–299, http://dx.doi.org/10.1016/j.jenvrad.2014.06.027.
Simons, M., Minson, S.E., Sladen, A., Ortega, F., Jiang, J., Owen, S.E., Webb, F.H., 2011. The 2011 magnitude 9.0 Tohoku-Oki earthquake: mosaicking the megathrust from seconds to centuries. Science (New York, N.Y.) 332 (6036), 1421–1425, http://dx.doi.org/10.1126/science.1206731.
Steinhauser, G., Brandl, A., Johnson, T.E., 2014. Comparison of the Chernobyl and Fukushima nuclear accidents: a review of the environmental impacts. Sci. Total Environ. 470–471, 800–817, http://dx.doi.org/10.1016/j.scitotenv.2013.10.029.
Stohl, A., Seibert, P., Wotawa, G., Arnold, D., Burkhart, J.F., Eckhardt, S., Yasunari, T.J., 2012. Xenon-133 and caesium-137 releases into the atmosphere from the Fukushima Dai-ichi nuclear power plant: determination of the source term, atmospheric dispersion, and deposition. Atmos. Chem. Phys. 12 (5), 2313–2343, http://dx.doi.org/10.5194/acp-12-2313-2012.
Tagami, K., Uchida, S., Uchihori, Y., Ishii, N., Kitamura, H., Shirakawa, Y., 2011. Specific activity and activity ratios of radionuclides in soil collected about 20 km from the Fukushima Daiichi Nuclear Power Plant: radionuclide release to the south and southwest. Sci. Total Environ. 409 (22), 4885–4888, http://dx.doi.org/10.1016/j.scitotenv.2011.07.067.
Walling, D.E., Quine, T.A., 1991. Use of 137Cs measurements to investigate soil erosion on arable fields in the UK: potential applications and limitations. J. Soil Sci. 42 (1), 147–165, http://dx.doi.org/10.1111/j.1365-2389.1991. tb00099.x.
Yamashiki, Y., Onda, Y., Smith, H.G., Blake, W.H., Wakahara, T., Igarashi, Y., Yoshimura, K., 2014. Initial flux of sediment-associated radiocesium to the ocean from the largest river impacted by Fukushima Daiichi Nuclear Power Plant. Sci. Rep. 4, 3714, http://dx.doi.org/10.1038/srep03714.
Yasunari, T.J., Stohl, A., Hayano, R.S., Burkhart, J.F., Eckhardt, S., Yasunari, T., 2011. Cesium-137 deposition and contamination of Japanese soils due to the Fukushima nuclear accident. Proc. Natl. Acad. Sci. U. S. A. 108 (49), 19530–19534, http://dx.doi.org/10.1073/pnas.1112058108.
Yasutaka, T., Naito, W., 2015. Assessing cost and effectiveness of radiation decontamination in Fukushima Prefecture, Japan. J. Environ. Radioact., http://dx.doi.org/10.1016/j.jenvrad.2015.05.012.